

Environmental Science Nano

Accepted Manuscript



This is an *Accepted Manuscript*, which has been through the Royal Society of Chemistry peer review process and has been accepted for publication.

Accepted Manuscripts are published online shortly after acceptance, before technical editing, formatting and proof reading. Using this free service, authors can make their results available to the community, in citable form, before we publish the edited article. We will replace this *Accepted Manuscript* with the edited and formatted *Advance Article* as soon as it is available.

You can find more information about *Accepted Manuscripts* in the [Information for Authors](#).

Please note that technical editing may introduce minor changes to the text and/or graphics, which may alter content. The journal's standard [Terms & Conditions](#) and the [Ethical guidelines](#) still apply. In no event shall the Royal Society of Chemistry be held responsible for any errors or omissions in this *Accepted Manuscript* or any consequences arising from the use of any information it contains.

Heteroaggregation of Bare Silver Nanoparticles with Clay Minerals

Jibin Liu, Yu Sik Hwang¹ and John J. Lenhart*

Department of Civil, Environmental and Geodetic Engineering

The Ohio State University, Columbus, OH 43210, United States

¹Future Environmental Research Center, Korea Institute of Toxicology, Jinju 660-844, Republic of Korea

Revised manuscript for submittal to: *Environmental Science: Nano*

August 2015

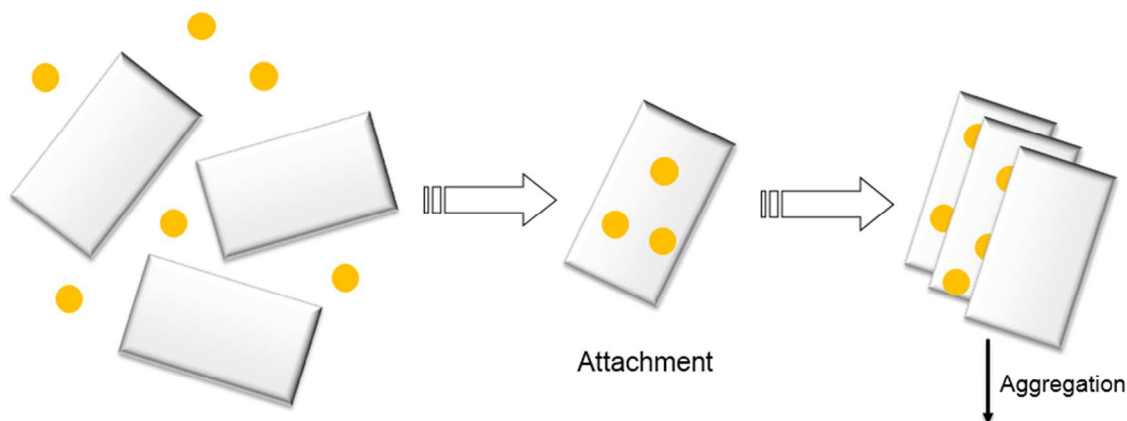
*Corresponding Author, Tel.: +1-614-688-8157; Fax: +1-614-292-3780.

Email: lenhart.49@osu.edu

Nano Impact Statement

Understanding how nanoparticles interact with other particulate material in aqueous systems is essential to assess the fate of nanoparticles because these interactions directly or indirectly affect nanoparticle form, concentration, and aggregation. Clays are one of the dominant naturally occurring particle classes in aqueous system. Thus, in this study we investigated the heteroaggregation of silver nanoparticles with two clay minerals in neutral pH solutions. Our results suggest the binary clay-nanosilver systems behave nearly the same as the clay-only systems under the experimental conditions studied. Thus, to account for the influence of native particles, such as clays, on the fate of silver nanoparticles in aqueous system may simply require the understanding of the aggregation behavior of the clay minerals.

TOC Artwork



1 **Abstract**

2 In this study, we investigated the heteroaggregation of silver nanoparticles with clay minerals in neutral
3 pH solutions as a function of electrolyte type and concentration. Bare nanoparticles with a nominal
4 diameter of 60.9 ± 0.5 nm were synthesized and their aggregation behavior with illite (IMt-2) and
5 montmorillonite (SWy-2), pretreated to obtain monocationic (Na-clay) and dicationic (Ca-clay)
6 suspensions, was studied. Aggregation was monitored as a function of electrolyte concentration in both
7 homo- and heteroaggregation scenarios by measuring the change in hydrodynamic diameter as a function
8 of time using dynamic light scattering. Our results did not show significant differences in the stability of
9 binary component systems of bare silver nanoparticle and clays at pH 7 when compared to the single
10 particle systems of clay or silver at the same pH. In each case, high electrolyte concentrations were
11 needed to overcome the energy barrier to form aggregates, which we attribute to weakly charged or
12 negatively charged clay edges, negatively charged silver nanoparticles, as well as the permanently
13 negatively charged basal plane surfaces of the clays at pH 7. The results suggest that a binary system of
14 clay (either montmorillonite or illite) and bare silver nanoparticles can be treated as a single component
15 system of the respective clay under the experimental conditions studied, and the fate of silver
16 nanoparticles in aqueous system may be controlled by their heteroaggregation with native particles, such
17 as clays.

18 Introduction

19 Engineered nanoparticles are intentionally produced particles with a size less than 100 nm. Owing to this
20 small size, the particles' properties are drastically different from those for the bulk material of the same
21 composition¹. As the application of nanotechnology has increased, many engineered nanoparticles have
22 been introduced to products used in our daily lives. Due to this fact, questions arise about nanoparticle
23 release to the environment during product use or disposal as well as the potential of these released
24 particles to cause adverse effects to the environment and human health^{1, 2}. Routes of entry to the
25 environment may originate from point sources such as factories, or from non-point sources such as wet
26 deposition, storm water runoff, and the degradation or disposal of discarded nanomaterial-containing
27 products³. In aqueous systems, the fate of engineered nanoparticles is controlled by physical transport
28 (e.g., advection or sedimentation), chemical or biological transformation (e.g., oxidation-reduction or
29 dissolution) and particle interaction (e.g., heteroaggregation) processes⁴. These processes can act
30 independently or mutually and their role in determining the fate of nanoparticles remains poorly
31 understood^{2, 3}. An accurate determination of fate is critical to determining the risk of nanoparticles to
32 humans, organisms, and the environment³.

33 Among metallic nanoparticles currently being produced and utilized, silver nanoparticles (AgNPs) are
34 unique in their widespread and extensive use in commercial products⁵. This reflects their utility as non-
35 specific antibiotics and thus they are utilized in products (e.g., clothing, food containers, wound dressings,
36 etc.) that exploit this effect for beneficial purposes⁶. When used, however, these products release
37 nanoparticles and these nanoparticles can be discharged into the environment⁶. The properties that make
38 AgNPs useful in commercial products could produce unforeseen adverse effects on aquatic biota and thus
39 there is considerable interest in determining the mechanisms and processes responsible for dictating
40 AgNP fate in different settings, such as aquatic environments⁷. One of the dominant processes affecting
41 the fate of AgNPs in aquatic systems is aggregation and recent research provides insight into the effects
42 of electrolyte type, ionic strength, coating layer and organic matter on the aggregation of AgNPs⁸⁻¹⁰. For
43 example, NaCl, NaNO₃, and CaCl₂ produce “dissolution-accompanied” aggregation of silver

44 nanoparticles, meaning the particles simultaneously aggregate and dissolve¹⁰. More dissolution occurred
45 in chloride-containing AgNPs suspensions and the aggregates formed had smooth continuous surfaces,
46 while discrete aggregates were formed in nitrate-containing suspensions¹⁰. Aggregation of AgNPs is a
47 function of the capping layer, with AgNPs coated with large organic molecules such as the surfactant
48 Tween resisting aggregation more than those coated with smaller organic molecules, such as citrate or
49 sodium dodecyl sulfate⁹.

50 While these and similar studies provide insight into the environmental fate of AgNPs, they do so
51 based on the analyses of model systems that do not necessarily correspond well with natural systems. For
52 example, these studies do not account for interactions that may arise between silver nanoparticles
53 introduced into a system and native particles that are already present in a system, a process termed
54 heteroaggregation. Heteroaggregates form between two or more dissimilar particles and
55 heteroaggregation is thus used to describe the stability of particle suspensions that contain more than one
56 type of particle which may differ in size, shape, surface charge, etc.¹¹. One of the more dominant native
57 particle types in aquatic systems are clay minerals¹² and thus an initial attempt to study the influence of
58 heteroaggregation on AgNPs should naturally start by characterizing interactions between AgNPs and
59 clay minerals.

60 Heteroaggregation has been researched for years and several studies have evaluated nanoparticles.
61 Yates et al.¹³, for example, determined that adding nano-sized silica particles (4.3–285 nm) to stable
62 alumina dispersions produced large aggregates that readily settled out. Cerbelaud et al.¹⁴ also found
63 heteroaggregates formed between submicrometer Al₂O₃ particles and SiO₂ nanoparticles as silica
64 nanoparticles depositing on the alumina particles produced attractive interactions between the now silica-
65 coated alumina particles. Since the two particles were oppositely charged, the resulting process was
66 conceptualized by the following two steps: 1) deposition of the silica nanoparticles on alumina particles
67 and 2) aggregation of the silica-covered alumina particles¹⁴. Comparable studies with AgNPs are limited
68 and have only recently been studied. In studying interactions between AgNPs and hematite Huynh et al.¹⁵
69 observed rapid heteroaggregation that far exceeded that for the single-particle systems. This result was

70 similar to that observed by Yates et al.¹¹ and Cerbelaud et al.¹² and is a reflection of the attractive
71 electrostatic interactions between the two particles in these systems. Zhou et al.¹² report similar results in
72 their study of the heteroaggregation of AgNPs with montmorillonite at pH 4 where the edge sites of the
73 clay carry a positive charge. However, at pH 8 they report that mixed montmorillonite-Ag system
74 aggregation behavior was little changed compared to those for the single-particle systems. They attribute
75 this observation to the repulsive electrostatics that exist between the AgNPs and the clay face and edge
76 sites observed faster aggregation in a binary system of AgNPs and montmorillonite.

77 In this study, two common clay minerals, montmorillonite and illite, were chosen to evaluate their
78 effects on the heteroaggregation of AgNPs. These minerals are both 2:1 type clays, with one octahedral
79 alumina sheet sharing oxygen atoms with two tetrahedral silica sheets¹⁶⁻¹⁸. Montmorillonite is distinct
80 from illite in its ability to expand when it contacts water due to it lacking strongly held potassium ions in
81 the interlayer region and thus its ratio of edge to basal plane sites is greater than illite¹⁴. The basal planes
82 of clay lamella carry a permanent negative charge due to isomorphic substitution of Si- and Al-ions for
83 ions of lower valence, while the charge of the lamella edge is pH-dependent because of pH-dependence in
84 the exposed >Al-OH and >Si-OH surface groups¹⁶. The edge is positively charged when the pH is below
85 the point of zero charge (PZC) of the exposed functional groups and negatively charged when the pH is
86 above the PZC^{16, 19-21}. Extensive experimentation on the aggregation of clay minerals (see Table S1)
87 shows their behavior follows expected trends and depends upon pH, electrolyte solutions, ionic strength,
88 and saturating cations^{16, 19-21}. In the case of montmorillonite and illite, the greater proportion of illite edge
89 sites to basal plane sites results in it exhibiting aggregation tendencies that vary with the nature of the
90 saturating cation¹⁴. Although the heteroaggregation of clay particles with other nanoparticles has been
91 studied^{22, 23}, except for the study of Zhou et al.¹² the aggregation of clay minerals with AgNPs remains
92 little understood.

93 The overall goal of our research is to elucidate the fundamental processes that control the fate of
94 silver nanoparticles in natural aquatic environments, with the specific objective of this study being to
95 evaluate the influence of heteroaggregation. We focus our attention in this paper on expanding progress

96 made toward understanding the heteroaggregation of silver nanoparticles with clay minerals presented by
97 Zhou et al.¹², by comparing results with two clay minerals (montmorillonite and illite) as a function of
98 saturating cation (Na^+ and Ca^{2+}) and electrolyte (NaCl , NaNO_3 or CaCl_2). Although montmorillonite and
99 illite are structurally similar, the non-expanding nature of illite produces aggregation behavior with
100 greater dependence on solution composition than that for montmorillonite (see Table S1). Thus, we
101 hypothesize that illite interactions with AgNPs will exhibit a greater dependence on solution composition
102 (e.g., saturating cation) than will montmorillonite. To facilitate comparisons to the conditions in this study
103 were the same as those previously used to evaluate the homoaggregation of silver nanoparticles¹⁰. Our
104 results did not show significant differences in the stability, as defined by the critical coagulation
105 concentration (CCC), of binary systems of silver nanoparticle and clays when compared to the single
106 component systems under the same conditions. They also did not exhibit much dependence on the clay
107 mineral or saturating cation, which was counter to our original hypothesis. Instead, the broader
108 aggregation behavior of the binary systems closely mimicked that for the clay minerals and thus we
109 propose under conditions present in natural systems (e.g., circumneutral pH and excess concentration of
110 natural particles) that the aggregation kinetics of binary systems with AgNPs and natural particles, such as
111 clays, can be approximated based upon knowledge of just the single component clay systems.

112

113 **Experimental Details**

114 **Materials**

115 AgNO_3 ($\geq 99.8\%$) and D-maltose monohydrate (99%) were purchased from Sigma-Aldrich and used as
116 received. Ammonium hydroxide (20-22% as NH_3 , trace metal grade) was bought from Fisher Scientific.
117 All other reagents were analytical grade or higher. All experiments used deionized water (Millipore Milli-
118 Q) with a resistivity of $18.2 \text{ M}\Omega\text{-cm}$. The electrolyte solutions (NaCl , NaNO_3 , and CaCl_2), buffer solution
119 (NaHCO_3), and solutions employed in silver nanoparticle synthesis were filtered through $0.1 \mu\text{m}$ cellulose
120 ester membranes (Millipore) before use. All labware and glassware were thoroughly cleaned and soaked

121 in 5% nitric acid for at least one day before use, followed by a thorough rinse with deionized water and
122 oven-drying. The labware was immediately used or stored in a dust-free environment prior to use.

123

124 **Clay Preparation**

125 Montmorillonite (SWy-2) and illite (IMt-2) were obtained from the Clay Minerals Society and prepared
126 as monocationic suspensions following established protocols^{24, 25}. To begin, 5g of each clay in 250mL
127 deionized water was rapidly mixed for 45 min. The less than 2 μm size fraction was isolated into the
128 supernatant by overnight gravity sedimentation. The supernatant was decanted and the electrolyte
129 concentration was adjusted to be 1M NaCl. For montmorillonite, this step was followed by a rapid 15
130 minute mix, whereas for illite the suspension was adjusted to pH 3 with 10% HCl and stirred for two
131 hours. The clays were separated from their respective suspensions through centrifugation at 3600 rpm for
132 30 min. The supernatant was decanted and fresh 0.01M NaCl was added. The clay suspensions were
133 vigorously shaken to re-suspend the clay particles and subsequently centrifuged once again at 3600 rpm
134 for 30min. This washing procedure was repeated 5 times. The suspensions were dialyzed against 0.01M
135 NaCl. The solution was changed daily until the conductivity of the clay suspension was the same as the
136 0.01M NaCl.

137 Calcium-saturated clay samples were prepared following the methods previously described with the
138 exception that NaCl was replaced with CaCl_2 . All of the clays were stored as concentrated suspensions in
139 the dark at 4 °C.

140

141 **Silver Nanoparticle Synthesis**

142 Monodisperse suspensions of silver nanoparticles were synthesized following Li et al.¹⁰. In short, 2 mL of
143 0.01M AgNO_3 was pipetted into a 50 mL glass beaker followed by 10 mL of 0.02M ammonium
144 hydroxide. The solution was stirred using a small Teflon-coated magnetic stir bar. The solution pH was
145 adjusted to ca. 11.5 through the addition of 250 μL of 0.1M NaOH, after which 8 mL of 0.025M D-
146 maltose was introduced to reduce the $\text{Ag}[(\text{NH}_3)_2]^+$ complex to form metallic silver nanoparticles. After

147 the addition of all reagents, the suspension was equilibrated for 30 min in the dark at room temperature
148 (20 ± 1 °C).

149 The freshly synthesized silver nanoparticles were dialyzed against deionized water using a cellulose
150 ester membrane (Spectra/Por, 8-10k MWCO) over a period of 24 hours. The deionized water was
151 changed a minimum of 4 times, which Li. et al.¹⁰ report is sufficient time to remove residual ions. Six
152 such batches of silver nanoparticles were synthesized and combined to form the stock suspension which
153 was stored in a polypropylene bottle in the dark at 4 °C. The concentration of the stock suspension,
154 determined using an inductively coupled plasma optical emission spectrometer (Varian Vista AX), was 60
155 mg-Ag/L which corresponds to an approximate yield of 55% of the initial Ag.

156

157 **Particle Characterization**

158 The hydrodynamic diameter and UV-vis spectrum of the silver nanoparticles was determined on a sample
159 that was diluted by 25 times in a sodium bicarbonate – sodium chloride buffer solution that maintained
160 the pH at 7.0 ± 0.3 and ionic strength at 1mM. The hydrodynamic diameter was measured by dynamic
161 light scattering (DLS) (90Plus, Brookhaven Instruments Corp., Holtsville, NY). The UV-vis spectrum
162 was collected over the wavelength range of 200 – 700 nm using a Shimadzu UV-4201PC UV-vis
163 spectrophotometer.

164 The morphology and size of the dispersed silver nanoparticles and clays were imaged using a Technai
165 G2 Spirit Transmission Electron Microscope (TEM) with a 120 kV electron beam. Samples were
166 prepared by placing one drop of the working suspension on a 100 mesh copper grid that was dried under
167 nitrogen. Samples of dispersed silver nanoparticles and clays were prepared using concentrated stock
168 suspensions which were sonicated before use. The morphology of the heteroaggregates was also
169 evaluated using the TEM, where one drop of the suspension generated from the heteroaggregation
170 experiments was used instead.

171 The electrophoretic mobility of Na-/Ca-montmorillonite and illite was measured by a Brookhaven
172 Instrument Corp. ZetaPALS instrument. The Smoluchowski equation was used to calculate the zeta

173 potential from the corresponding mobility values for a particle of arbitrary shape with a nominal diameter
174 that is much larger than the thickness of the electrical double-layer²⁶. The measurements were conducted
175 at a temperature of 22 ± 0.5 °C across the pH range of 4.0 - 10.0 in 1mM NaCl solutions. The samples
176 were equilibrated for 5 min and for each pH value the data comprised ten individual measurements
177 collected and averaged for three separate samples. The effects of NaCl (0.1mM – 10mM) and CaCl₂
178 (1mM – 500mM) on the electrophoretic mobility of the clay minerals were evaluated as well at pH 7.

179 **Aggregation Kinetics**

180 Aggregation kinetics for both the homoaggregate and heteroaggregate systems was determined by
181 measuring the initial time rate of change in the average hydrodynamic radius of the particle suspensions
182 using DLS. The instrument was equipped with a 678 nm laser with a detection angle of 90 degrees and
183 the experiments were conducted at a temperature of 22 ± 0.5 °C.

184 All working suspensions were prepared by diluting stock suspensions in a 0.05 mM sodium
185 bicarbonate buffer at pH 7.0 ± 0.3 . Individual particle concentrations were kept the same for both the
186 homoaggregation and heteroaggregation experiments. This entailed diluting the stock particle suspensions
187 when preparing the working suspensions for the heteroaggregation experiments with a particle
188 concentration twice that for the homoaggregation experiments (see Table S2). All working suspensions
189 were briefly sonicated in an ultrasonic water bath before each experiment.

190 For the homoaggregation experiments, 3 mL of the particle suspension of interest was pipetted into a
191 disposable acrylic cuvette. The cuvette was prepared before use by washing using 5% HNO₃ followed by
192 a thorough rinse with deionized water. Predetermined amounts of electrolyte and buffer solutions were
193 added to the cuvette to obtain the desired ionic strength, while maintaining the total volume at 4 mL. The
194 cuvette was covered with a plastic lid, quickly hand-shaken and inserted into the DLS sample holder. The
195 heteroaggregation experiments were the same except that 1.5 mL of silver nanoparticles and 1.5 mL of
196 the clay suspensions of interest were used. In either case, measurements begun immediately upon
197 inserting the cuvette into the DLS. For silver nanoparticle systems, measurements were collected over a

198 period of 15 min with 90s intervals between measurements, while single clay and binary component
199 systems were measured over a period of 5 min with 30s intervals between measurements.

200 The stability of the suspensions was analyzed by comparing variations in the inverse stability ratio
201 ($1/W$) with ionic strength where $1/W$ is defined as the ratio of the experimental aggregation rate constant
202 (k_{exp}) to that determined for rapid aggregation (k_{rapid}), or diffusion-limited aggregation, as shown in the
203 following expressions²⁷:

$$204 \quad k_{exp} = \frac{1}{aNr_0} \frac{dr}{dt} \quad (1)$$

$$205 \quad \frac{1}{W} = \frac{k_{exp}}{k_{rapid}} \quad (2)$$

206 where N is the initial particle concentration, r_0 is the initial particle radius, and a is an optical factor. The
207 k_{exp} value was calculated by conducting a linear least-squares regression analysis on the time-rate of
208 change of the hydrodynamic radius (dr/dt), while the k_{rapid} value was determined as the average value of
209 the k_{exp} values under diffusion-limited aggregation conditions. This latter value was specific to each
210 homoaggregation or heteroaggregation system and electrolyte. The relationship between $1/W$ and ionic
211 strength was used to identify the critical coagulation concentration (CCC) for each system and it was
212 determined as the intersection point of two straight lines that represent the change of $1/W$ as a function of
213 ionic strength in the reaction and diffusion-limited aggregation regimes, respectively²⁶.

214

215 **Results and Discussions**

216 **Silver Nanoparticle Characterization**

217 The hydrodynamic diameter of the silver nanoparticles determined by DLS was 60.9 ± 0.5 nm. TEM
218 images show the silver nanoparticles' morphology as smooth and roughly spherical with a diameter
219 similar to that measured by DLS (Figure S1a). Based on this size, the concentration of the stock
220 suspension (60 mg Ag L^{-1}), and the density of metallic silver (10.5 g cm^{-3}), we calculated a particle
221 concentration for the stock suspension of 5×10^{10} particles mL^{-1} . Based on the dilutions used to prepare

222 working solutions (see Table S2), the silver nanoparticle concentration used in aggregation experiments
223 was 1.5×10^9 particles mL^{-1} .

224 The UV-vis spectrum (Figure S1b) of freshly synthesized silver nanoparticles showed a maximum
225 absorption peak at a wavelength of 433 nm, which was consistent with the reported location of the surface
226 plasmon absorption band of silver nanoparticles synthesized using this method²⁸. The observed red-shift
227 in the position of the absorption peak compared to that for monodispersed silver nanoparticles with a
228 diameter below 100 nm with no adsorbed or oxidized layer, as well as the broadening of the absorption
229 band provide evidence for the existence of an oxidized layer on the particle surface¹⁰.

230 According to Li. et al.¹⁰, the silver nanoparticles synthesized with this method have a negative zeta
231 potential across the pH range of 4.0 to 10.0 that remains relatively unchanged at -45.8 ± 0.9 mV in 1 mM
232 NaCl. Li et al.¹⁰ rationalize the measured negatively charged surfaces may reflect the existence of an
233 oxide surface layer and the adsorption of anions during synthesis. Increasing the electrolyte concentration
234 or valence of the electrolyte cation decreased the magnitude of the zeta potential¹⁰, reflecting the increase
235 in charge screening under these conditions.

236

237 **Clay Mineral Characterization**

238 *Characterization of Montmorillonite*

239 The diameter of dispersed montmorillonite lamellae ranged from 200 nm to 700 nm (Figure S2a),
240 consistent with the method of preparation²⁴. From the DLS measurement of the suspensions, however,
241 the most predominant hydrated particle size for both forms of montmorillonite was ca. 200 nm. This size
242 reflects the implied assumption that the particles were spherical as DLS determines the rotationally
243 averaged particle size. Particle sizes determined using DLS are more sensitive to the major dimension of
244 the particle than they are to the minor dimension and thus we were not able to discern any differences in
245 thickness of the clay lamella for Na- or Ca-montmorillonite. According to Schramm and Kwak²⁹ these
246 differences are on the order of ca. 5, with Ca-forms of the clay being thicker. The concentrations of the
247 Na- and Ca-montmorillonite (Na-MONT and Ca-MONT) stock suspensions were determined by

248 gravimetric analysis as 25 g L^{-1} and 41 g L^{-1} , respectively. Using the spherical size determined from DLS
249 for these particles of 200nm and a density of 2.35 g cm^{-3} we estimated particle concentrations in our stock
250 clay suspensions of ca. 3×10^{15} particles mL^{-1} for Na-MONT and 4×10^{15} particles mL^{-1} for Ca-MONT.
251 The assumption of a spherical dimension may result in a lower particle concentration since it does not
252 represent the true particle size or morphology. Based upon the dilutions used (see Table S1), the
253 concentration of Na-MONT in the aggregation experiments was 7.6×10^9 particles/mL and that for Ca-
254 MONT was 6.3×10^9 particles/mL.

255 The zeta potential of the sodium- and calcium-forms of the montmorillonite in 1 mM NaCl remained
256 unchanged at $-46.5 \pm 7.14 \text{ mV}$ and $-22.6 \pm 2.88 \text{ mV}$, respectively, across the pH range 4.0 to 10.0 (Figure
257 1). These results were consistent with those published for this montmorillonite suspended in NaCl^{12, 30}.
258 Under the experimental conditions studied, the zeta potential of Ca-montmorillonite was less negative
259 than that for Na-montmorillonite. Montmorillonite has a higher affinity for Ca^{2+} than Na^+ and the bound
260 Ca^{2+} can suppress the negative charge of the basal planes^{30, 31}. Given time, the bound Ca^{2+} could be
261 displaced when Ca-montmorillonite was dispersed in NaCl, but since the electrolyte concentration (1mM)
262 was too low and the time during sample preparation (less than 30 min) was too short such ion exchange
263 was not fully completed³⁰.

264 The zeta potential of both forms of montmorillonite were measured across the NaCl and CaCl_2
265 concentrations corresponding to those studied in the aggregation experiments (Figure 2a). At low
266 electrolyte concentration, the zeta potential for Ca-montmorillonite was less negative than that for Na-
267 montmorillonite. As the electrolyte concentration increased, however, the zeta potential for both forms of
268 the clay converged to similar values. The same trend existed for both CaCl_2 and NaCl. It was more
269 pronounced for NaCl, however, as the zeta potential of Na-montmorillonite became less negative as NaCl
270 increased from 30mM to 500mM. Likely, this just reflects compression of the electrical double layer at
271 elevated electrolyte concentration²⁶. Below 30 mM NaCl, the absolute value of the zeta potential of Na-
272 montmorillonite increased from ca. 40mV to ca. 65mV. According to Delgado et al.³² this reflects
273 montmorillonite can undergo rapid hydrolysis at circumneutral pH, whereby H^+ , exchanged for bound

274 Na^+ , induces the release of Al^{3+} and Mg^{2+} from montmorillonite which could produce the observed
275 increase in the magnitude of the zeta potential. Hydrolysis is distinct from mineral dissolution, which
276 occurs slowly (e.g., Metz et al.³³), and is partially driven by the accumulation of H^+ at the clay interface
277 needed to satisfy electroneutrality in the system^{23,24}. Delgado et al.³² described this hydrolysis as two steps:
278 (1) a rapid exchange of hydrogen ions in the solution with Na^+ originally attached to the montmorillonite
279 and (2) a slow penetration of the exchanged H^+ into the sheets of montmorillonite. The penetrating
280 hydrogen ions induce the release of Al^{3+} and Mg^{2+} from montmorillonite into the solution. The released
281 multivalent cations could also compress the electrical double layer which would reduce the magnitude of
282 zeta potential. At the same time, however, the loss of these cations would decrease the zeta potential of
283 montmorillonite. The determination of the electrophoretic mobility, hence zeta potential, is also
284 influenced by the high surface conductivity of montmorillonite which is reported to also produce low
285 absolute values under dilute electrolyte conditions³⁴. Thus, the observed decrease of zeta potential of clay
286 was likely the net result of these combined actions. The hydrolysis process is kinetically hindered at
287 elevated electrolyte concentrations and thus it tends to be observed at electrolyte concentrations less than
288 10^{-3} M ^{32, 35, 36}. Callaghan and Ottewill³⁷ and Rossi et al.³⁸ observed different trends in the zeta potential
289 that entailed a decrease (increase in the magnitude) at NaCl concentrations above 10^{-2} M . Rossi et al.³⁸
290 attribute this to particle dissolution and ion release. Finally, aggregation of the montmorillonite during
291 the five minute equilibration time prior to the zeta potential determinations was possible, particularly at
292 electrolytes equal to or greater than 30 mM, and it could also have influenced these measurements.
293 Considering the obvious sensitivity of clay surfaces to methods of preparation and storage³⁶, our results
294 were similar in magnitude to those previously reported.

295 When Ca-montmorillonite was suspended in 1 to 30 mM NaCl , a similar trend of decreasing zeta
296 potential with increasing NaCl concentration resulted. However, in this case the origin of the trend not
297 only reflects hydrolysis and surface conductance, but also the exchange of Ca^{2+} bound to the clay with
298 Na^+ ions in the solution. This net loss of bound cation charge could produce a lower zeta potential. The
299 time needed for complete replacement of Ca^{2+} by Na^+ is reported to be around 24 h³⁶ and presumably

300 given sufficient time the two data sets would converge. Since the equilibration time was much less than
301 24 hours, Ca-montmorillonite had a consistently higher (less negative) zeta potential than did Na-
302 montmorillonite.

303 In systems with CaCl_2 , the zeta potential for Na-montmorillonite increased as the electrolyte
304 concentration increased (Figure 2a). This reflects both the exchange of bound Na^+ with solution phase
305 Ca^{2+} and the enhanced compression of the electrical double layer induced by the divalent calcium cations.
306 However, except for an increase in the standard error of the zeta potential with increasing electrolyte, no
307 significant change in the zeta potential of Ca-montmorillonite was observed in the range of 10^{-4} to 10^{-2} M
308 CaCl_2 (Figure 2a). While the reason for this result was not known with certainty, it was similar to results
309 presented in the literature³⁹ and may reflect the influence of particle aggregation during the preparation of
310 the samples prior to these measurements .

311

312 *Illite Characterization*

313 The illite flakes ranged in size from roughly 50 to 200 nm and differed from montmorillonite in that illite
314 had irregular and curved outlines (Figure S2b). In some locations, individual illite lamella appeared to
315 orient perpendicular to the imaging plane, and the resulting cluster of illite flakes formed a wheel-like
316 formation. This wheel-like structure indicates an edge-to-face orientation of illite which allows small
317 angles between each flake (sub-parallel orientation). Similar images exist for illite in both distilled and
318 saline water⁴⁰. Except for these mostly isolated wheel-like formations, it appeared that the majority of the
319 illite was oriented face-to-face. The concentrations of Na- and Ca-illite in the respective stock
320 suspensions were 1.2 g L^{-1} and 3.6 g L^{-1} . Following the approach used for montmorillonite, a density of
321 2.75 g cm^{-3} and diameters measured from DLS of 135 nm for Na-illite and 270 nm for Ca-illite we
322 estimated particle concentrations in our stock clay suspensions of ca. 3×10^{14} particles mL^{-1} and 1×10^{14}
323 particles mL^{-1} , respectively. Based upon the noted dilutions (see Table S1), the concentration of Na-illite
324 in the aggregation experiments was 5.1×10^9 particles/mL and that for Ca-illite was 3.6×10^9

325 particles/mL. As previously noted, the assumption of a spherical particle likely resulted in an
326 underestimate of the illite particle concentration.

327 At pH 7, the zeta-potential of Na-illite was $-44 \pm 4\text{mV}$ while for Ca-illite it was $-21 \pm 2\text{mV}$ (Figure 1).
328 Similar trends were found for the zeta-potential of illite in the pH range 4 to 10 as was measured for
329 montmorillonite. This was expected considering both clay minerals had the same basic structure. As was
330 observed for montmorillonite, the calcium-form of illite had a less negative zeta potential than did the Na
331 form, reflecting the presence of the bound divalent cations.

332 The zeta potential for both Na- and Ca-illite generally increased (trend to a less negative value) as the
333 NaCl concentration increased from 1mM to 500mM (Figure 2b). Unlike what was observed for Na-
334 montmorillonite, however, no significant decrease in the zeta potential occurred for Na-illite below 30
335 mM NaCl. Illite is a nonexpanding clay⁴¹ and although the 2:1 layer structure is similar to that for
336 montmorillonite, the cation exchange capacity (CEC) of illite is lower than that of montmorillonite³⁹. The
337 CEC of the montmorillonite in this study is $1040 \text{ mmol kg}^{-1}$ ²⁴, while that for illite is 231 mmol kg^{-1} ²⁵,
338 reflecting the smaller amount of internal cations (i.e., potassium ions) available for release from illite than
339 montmorillonite⁴². Thus, the decrease in the magnitude of the negative zeta potential as NaCl was
340 increased from 1 mM to 500 mM likely reflects compression of the electrical double layer induced by the
341 increasing electrolyte. Similar to Ca-montmorillonite, the exchange of clay-bound Ca^{2+} associated with
342 Ca-illite with solution-phase Na^+ remains possible and if it occurred it could have produced the reduction
343 in the magnitude of the zeta potential at NaCl below 30 mM.

344 The effect of CaCl_2 on the zeta potentials of both Na- and Ca-illite (Figure 2b) reveals illite has a
345 higher affinity for Ca^{2+} than Na^+ . Since illite is a nonexpanding clay, suspending Na-illite in CaCl_2 was
346 assumed to lead to more rapid and complete exchange of Na^+ with Ca^{2+} than that for Na-montmorillonite.
347 As a result, the zeta potential of Na-illite was very close to that for Ca-illite from 1mM to 10mM CaCl_2 .

348

349 **Homoaggregation of Single Component Systems**

350 *Homoaggregation of Silver Nanoparticles*

351 The aggregation behavior for the silver nanoparticles exhibited trends consistent with that previously
352 observed^{8c} to indicate coincident particle dissolution and particle aggregation (Figures 3a and 3b). In the
353 monovalent electrolyte solutions, the initial particle diameter decreased as the electrolyte concentration
354 increased from 10mM to 200mM. However, since the dissolution of silver nanoparticles was
355 accompanied by aggregation, this initial decrease in size was soon followed by an overall increase with
356 time as aggregation of the particles proceeded. Li. et al.¹⁰ reported the size decrease to be the result of the
357 dissolution of an oxidized surface layer evident in the absorption spectrum (see Figure S1b). According to
358 Li et al.¹⁰, this reaction is influenced by the concentration and type of electrolyte. When the electrolyte is
359 NaCl, AgCl_(s) precipitates on the nanosilver particle surface, resulting in a modification of the silver
360 nanoparticles morphology¹⁰. NaNO₃, however, did not produce a precipitate nor did it change aggregate
361 morphology¹⁰. Regardless, the aggregation of nanosilver in these two electrolytes was similar (Figures 3a
362 and 3b) and was consistent with other data presented in the literature^{10, 43, 44}. In our experiments, the CCC
363 of silver nanoparticles in NaCl was ca. 40mM, while it was ca. 35mM in NaNO₃. These results were
364 consistent with those presented by Li. et al.^{10, 43, 44} indicating the AgNPs synthesized in these experiments
365 behaved similarly to those in previous studies.

366 When the electrolyte was CaCl₂ the CCC of silver nanoparticles was much lower (ca. 2mM) than that
367 in NaCl/NaNO₃ (Figure 4). According to the Schulze-Hardy rule²⁶, $CCC_{[Na]}/CCC_{[Ca]}$ equals z^6 for particles
368 with a large zeta potential ($|\xi| > 50\text{mV}$), and z^2 for those with a low zeta potential ($|\xi| < 50\text{mV}$), where z is
369 the counterion charge (i.e., $z = 2$ in the case of Ca²⁺). In our experiments, the ratio of $CCC_{[Na]}$ and $CCC_{[Ca]}$
370 was approximately proportional to z^4 . This intermediate value between the two predicted by the Schulze-
371 Hardy rule (i.e., z^6) is consistent with previous measurements, and according to Li et al.^{9, 10} indicates the
372 modification of surface charge due to the adsorption of cations on the surface of the silver nanoparticles.

373

374 *Homoaggregation of Montmorillonite*

375 Although the trends in zeta potential for sodium-saturated montmorillonite did not exhibit typical trends
376 (Figure 2a), the aggregation kinetics did approximate Derjaguin-Landau-Verwey-Overbeek (DLVO) type

377 aggregation kinetics (Figure 5a). DLVO-type aggregation refers to aggregation controlled by the
378 combined influence of electrostatics and van der Waals interactions^{45, 46}. At low electrolyte
379 concentrations (e.g., 1 - 50 mM NaCl or 0.5 - 1 mM CaCl₂), an increase in the electrolyte concentration
380 led to a corresponding increase in the aggregation rate (Figure 5a). Above these electrolyte concentrations,
381 the aggregation rate reached a maximum value that did not significantly vary as the electrolyte
382 concentrations increased. For a monovalent electrolyte, similar CCC values of ca. 50 mM were
383 determined for Na-montmorillonite in NaCl and NaNO₃ (Figure 5a). This CCC value was comparable to
384 those reported by Tombácz et al., of ca. 25, 50, and 100 mM NaCl at pH 4, 6.5, and 8, respectively¹⁹. The
385 pH of 6.5 approximates the PZC of clay edges¹² where the edge transitions between positive and negative
386 charged states¹⁹. When the pH is below the PZC of the edge, the clay edge is positively charged and its
387 interaction with the negatively charged clay face becomes significant and decreases the stability of the
388 montmorillonite suspension. When the pH is above the PZC of the edge, both the edge and basal plane of
389 the clays are negatively charged edge-face interactions are limited resulting in an increase in the stability
390 of the suspension. Thus, our montmorillonite CCC at pH ~ 7 was similar to that reported in the literature
391 at a similar pH value, which is near the PZC of the clay edge.

392 In CaCl₂, the CCC value of Na-montmorillonite was estimated at 1.5 mM (Figure 5a). The ratio of the
393 CCC_[Na]/CCC_[Ca] was 33:1, proportional to z^5 , which was similar with that predicted by the Schulze-Hardy
394 rule of z^6 ⁴⁷. The difference could reflect the difficulty in preparing a pure monocationic montmorillonite
395 due to the potential release of multivalent cations (Mg²⁺, Al³⁺) from the clay minerals⁴⁷. It could also
396 reflect exchange of surface cations with the added electrolyte cation during aggregation^{31, 48}.

397 The same CCC of ca. 50 mM NaCl or NaNO₃ and ca. 2mM CaCl₂ were observed for both Na-
398 montmorillonite and Ca-montmorillonite at pH ~7 (Figure 5b). The cation used to saturate the basal
399 surface planes of montmorillonite had little to no impact on the suspension stability (Figure S3), which
400 was consistent with the similar values of zeta potentials for Na- and Ca-montmorillonite (Figure 2a). The
401 ratio of CCC_[Na]/CCC_[Ca] for Ca-montmorillonite was 25:1, or approximately $z^{4.6}$, which was close to that
402 of Na-montmorillonite. A similar result was obtained by Tombácz et al.³¹ and as a result they

403 hypothesized that montmorillonite aggregation depends only on the electrolyte, not the original cations
404 present in the montmorillonite. This was also consistent with the reported CCC of 70 mM for Mg-
405 montmorillonite at pH 7 in KCl⁴⁹.

406

407 *Homoaggregation of Illite*

408 Typical two-regime, DLVO-type aggregation kinetics were also observed for Na- and Ca-illite in NaCl,
409 NaNO₃ and CaCl₂ (Figure 6a and 6b). CCCs of ca. 70mM NaCl or NaNO₃ and ca. 2mM CaCl₂ were
410 determined for Na-illite at pH 7, while for Ca-illite the values were ca. 50mM NaCl or NaNO₃ and ca.
411 1mM CaCl₂. Literature data for Na-illite aggregation at neutral pH conditions is limited and quite variable
412 with reported CCC values of Na-illite varying from 7 to 40 mM NaCl at pH 7^{21, 47, 50, 51}. This variation
413 likely reflects the different illite sources and sample preparation. For example, Hesterberg et al.²¹ prepared
414 their sample by first washing it with concentrated NaClO₄ and KClO₄ solutions, followed by a
415 NaClO₄/HClO₄ wash at pH 3.5 and then concluding with equilibration in NaClO₄. The KClO₄ was used to
416 maintain the illite's structural K. In the end, their illite samples prepared as stock suspension at pH 7
417 contained residual Na⁺ and K⁺. These residual ions may have decreased the CCCs of illite samples in their
418 experiments, as they reported a CCC of 30mM NaClO₄ at a pH of 7.5. Only homoionic aggregation data
419 is available for Ca-illite⁵², with a CCC value for Ca-illite of < 0.5mM CaCl₂. Based on these results, the
420 ratios of CCC<sub>[Na]}/CCC[Ca] for both the Na- and Ca-illite were $z^{5.13}$ and $z^{5.64}$, respectively. These were
421 close to those estimated from the Schulze-Hardy rule, with differences again possibly reflecting the
422 release of residual cations from the clays⁴⁷.</sub>

423 Similar to montmorillonite, the bound cation had little effect on the stability of illite (Figure S4). The
424 CCCs of Ca-illite and Ca-montmorillonite were similar, but the CCCs of Na-illite were slightly higher
425 than those for Na-montmorillonite (Table 1). Oster et al.⁴⁷ similarly observed the CCC of Na-illite was
426 higher than the CCC for Na-montmorillonite, while the CCCs of the two calcium forms of the clays were
427 similar. They concluded the irregular surfaces and terraced planar orientation (i.e., wheel-like orientation
428 in the TEM image of Na-illite in Figure S2b) of Na-illite lead to smaller edge-to-face attraction forces,

429 and eventually a higher CCC for Na-illite than for Na-montmorillonite. At the same time, the PZC of illite
430 ranges from 3.5 to 4.5⁵³⁻⁵⁵ and thus considering its structure is similar to montmorillonite a higher CCC
431 value of illite than that of montmorillonite seems reasonable.

432

433 **Heteroaggregation of Binary Component Systems**

434 *Silver Nanoparticles and Montmorillonite*

435 The stability of the mixed silver nanoparticle and montmorillonite (either Na- or Ca-saturated) systems as
436 measured based on the position of the CCC was little changed compared to that for the single-particle
437 systems (Figure 7). At neutral pH, both the edge and the face of the montmorillonite flakes were
438 negatively charged¹⁹. The silver nanoparticles were also negatively charged under these conditions¹⁰. As a
439 result the aggregation behavior assumed a form characteristic of typical two-regime aggregation. TEM
440 imaging (Figure 8) of the mixture in 100mM NaCl indicates the silver nanoparticles self-aggregation was
441 limited, particularly when compared with that expected for 100 mM NaCl (see Li et al. ¹⁰) and that many
442 were associating with the basal planes of the montmorillonite, but not the edges. This was consistent with
443 the negatively charged edge on the montmorillonite repelling the negatively charged silver nanoparticles.
444 The basal plane, while also negatively charged, was saturated with either Na⁺ or Ca²⁺ ions which could
445 attract the silver nanoparticles⁵⁶. Images collected at 10 mM NaCl not only indicate limited silver
446 nanoparticle self-aggregation, but also more limited interactions between the silver nanoparticles and the
447 clay minerals, as images collected showed the clay was devoid of deposited silver nanoparticles as well as
448 isolated silver nanoparticles (see Figure S6).

449 The rates of particle heteroaggregation at high electrolyte concentrations appeared to be dominated by
450 montmorillonite as the values for k_{rapid} for the binary-particle systems were similar to those for the
451 respective clay system as opposed to that for the silver nanoparticle system (See Tables S3 and S4). At
452 low electrolyte concentrations, however, the aggregation rates were intermediate between the two single
453 particle systems resulting in values for $1/W$ in the binary system being lower than those for either of the
454 single particle systems (e.g., see Figure 7a). These trends could reflect that the montmorillonite flakes

455 were roughly five times larger than the silver nanoparticles (Figures S1a and S2a) and the particle number
456 of montmorillonite was greater than that of the silver nanoparticles. It could also reflect non-DLVO
457 depletion force interactions that can form in binary systems that have a large ratio in particle sizes¹² when
458 the large particles are suspended in a dilute solution of the smaller ones⁵⁷. It occurs when the distance
459 between two large particles is less than the diameter of the smaller particles resulting in the small particles
460 being pushed out to leave a “free volume” between the large particles. This “free volume” will then lead
461 to an imbalance of pressure around the large particles, which in turn may form either attractive or
462 repulsive forces between these same particles⁵⁸. The attractive form of the depletion force can lead to the
463 flocculation of particles⁵⁷. The limited change in the stability of the mixture compared to the clay-only
464 system suggests any such depletion force was negligible, if present at all, in this binary system.

465 Thus, we propose that as electrolyte concentrations approach the CCC for the respective binary
466 system that the heteroaggregation of silver nanoparticles and montmorillonite was comprised of two
467 simultaneous processes. The first entailed the deposition of the silver nanoparticles onto the
468 montmorillonite flakes, likely during the initial stage of the experiment⁵⁹. In essence, montmorillonite acts
469 as a mobile collector in a manner that is analogous to the deposition of silver nanoparticles onto the
470 surface of sand⁶⁰ or silica⁶¹ where silver nanoparticle deposition occurs at ionic strength values as low as
471 5 mM^{42,43}. Since both the basal planes and the edges of montmorillonite were negatively charged at pH 7
472 as were sand⁴² and silica⁴³ their interactions with the silver nanoparticles should be similar. Based on the
473 size of nanoparticles (~60nm) and clay particles (200 – 400nm), however, it seems more likely that the
474 basal planes of the clay particles provide sites for nanoparticle deposition. The second process involved
475 the aggregation of the combined NP-clay particles, which aggregate more or less at the same rate as that
476 for the clay-only systems. Because of the larger particle number concentration of montmorillonite, the
477 deposition of bare silver nanoparticles appears to have little effect on its stability as the CCC of the
478 heteroaggregate system was similar to that for the clay-only system.

479
480 *Silver Nanoparticles and Illite*

481 The stability of the mixture of silver nanoparticles and illite (either Na- or Ca-form) was also little
482 changed from that for the single-particle systems (Figure 9). Illite has negatively charged edge and basal
483 planes at pH 7 according to the reported PZC value of 3.5⁵⁵ and thus as hypothesized for the binary
484 system with montmorillonite, these results also suggests the nano-sized silver first associated with the
485 basal illite face and then its fate was bound to the subsequent aggregation of the clay⁵⁹. We were unable to
486 collect images for these systems, but this proposed interaction between illite and the silver nanoparticles
487 seems reasonable due to the large particle size and higher number concentration of illite in these systems
488 compared to that for the silver nanoparticles.

489

490 **Conclusions**

491 Our results did not show significant differences in the stability of binary component systems of silver
492 nanoparticle and clays at pH 7 when compared to the single particle systems at the same pH. We attribute
493 this to weakly charged or negatively charged clay edges, as well as permanently negatively charged basal
494 plane surfaces of the clays at pH 7, thus all six combinations between silver nanoparticles and the clays in
495 binary systems (i.e., face-to-face, face-to-edge, edge-to-edge, nanoparticle-to-nanoparticle, face-to-
496 nanoparticle, edge-to-nanoparticle) are barrier-controlled (i.e., high electrolyte concentration is needed to
497 overcome the energy barrier to form aggregates). Our expectation for greater dependence in illite
498 aggregation on solution chemistry was also not evident in our experiments. While we cannot completely
499 neglect possible non-DLVO forces that arise from size asymmetry, such as depletion forces, the lack of
500 differences observed in the single- and binary-particle systems suggests their influence under the
501 conditions studied was negligible. Our results suggest under neutral pH and moderate to elevated
502 electrolyte concentrations approaching the measured CCC values that binary systems of
503 montmorillonite/illite and silver nanoparticles can be treated as single component clay systems. Further
504 research specifically highlighting conditions where the silver nanoparticles interact with clay phases and
505 the role of additional complexities such as natural organic matter are needed in order to better extend our
506 observations to predict the fate of silver nanoparticles in natural systems.

507

508 **Acknowledgements**

509 This study was supported under the research project Environmental Risk Assessment of Manufactured
510 Nanomaterials (KK-1403-02) funded by the Korea Institute of Toxicology (KIT) and done in
511 collaboration with the Department of Civil, Environmental and Geodetic Engineering (CEGE) at The
512 Ohio State University, Columbus, Ohio. The authors gratefully acknowledge the assistance of Ms. Elsa
513 Burrow, Ms. Yen-Ling Liu and Mr. Matthew Noerpel (all CEGE) for their assistance in this research. We
514 also acknowledge Dr. Xuan Li, US EPA, Cincinnati, OH, for his assistance and guidance in the
515 preparation and characterization of the silver nanoparticles. The images presented were generated using
516 instruments and services at The Ohio State University Campus Microscopy and Imaging Facility.
517 Electrophoretic mobility measurements were conducted at the Nanotech West Laboratory at The Ohio
518 State University.

519

520 **References**

- 521 1. M. Auffan, J. Rose, J. Y. Bottero, G. V. Lowry, J. P. Jolivet and M. R. Wiesner, *Nature*
522 *nanotechnology*, 2009, **4**, 634-641.
- 523 2. V. L. Colvin, *Nature Biotechnology*, 2003, **21**, 1166-1170.
- 524 3. M. R. Wiesner, G. V. Lowry, P. Alvarez, D. Dionysiou and P. Biswas, *Environmental*
525 *science & technology*, 2006, **40**, 4336-4345.
- 526 4. A. Praetorius, M. Scheringer and K. Hungerbuhler, *Environmental science & technology*,
527 2012, **46**, 6705-6713.
- 528 5. D. Rejeski, Nanotechnology and consumer products,
529 http://www.nanotechproject.org/publications/archive/nanotechnology_consumer_products/,
530 (accessed June, 2014).
- 531 6. T. M. Benn and P. Westerhoff, *Environmental science & technology*, 2008, **42**, 4133-
532 4139.
- 533 7. B. Nowack and T. D. Bucheli, *Environmental pollution*, 2007, **150**, 5-22.
- 534 8. X. Li and J. J. Lenhart, *Environmental science & technology*, 2012, **46**, 5378-5386.

- 535 9. X. Li, J. J. Lenhart and H. W. Walker, *Langmuir : the ACS journal of surfaces and*
536 *colloids*, 2012, **28**, 1095-1104.
- 537 10. X. Li, J. J. Lenhart and H. W. Walker, *Langmuir : the ACS journal of surfaces and*
538 *colloids*, 2010, **26**, 16690-16698.
- 539 11. A. Islam, B. Chowdhry and M. Snowden, *Advances in colloid and interface science*,
540 1995, **62**, 109-136.
- 541 12. D. Zhou, A. I. Abdel-Fattah and A. A. Keller, *Environmental science & technology*, 2012,
542 **46**, 7520-7526.
- 543 13. P. D. Yates, G. V. Franks, S. Biggs and G. J. Jameson, *Colloids and Surfaces A:*
544 *Physicochemical and Engineering Aspects*, 2005, **255**, 85-90.
- 545 14. M. Cerbelaud, A. Videcoq, P. Abélard, C. Pagnoux, F. Rossignol and R. Ferrando,
546 *Langmuir : the ACS journal of surfaces and colloids*, 2008, **24**, 3001-3008.
- 547 15. K. A. Huynh, J. M. McCaffery and K. L. Chen, *Environ. Sci. Technol. Lett.*, 2014, **1**,
548 361-366.
- 549 16. E. Tombácz and M. Szekeres, *Applied Clay Science*, 2006, **34**, 105-124.
- 550 17. M. Bentabol, M. D. Ruiz Cruz, F. J. Huertas and J. Linares, *Clay Minerals*, 2003, **38**,
551 161-172.
- 552 18. S. Laribi, B. Jouffrey and J.-M. Fleureau, *The European Physical Journal Applied*
553 *Physics*, 2007, **39**, 257-265.
- 554 19. E. Tombácz and M. Szekeres, *Applied Clay Science*, 2004, **27**, 75-94.
- 555 20. S. Goldberg and R. A. Glaubig, *Clays and Clay Minerals*, 1987, **35**, 220-227.
- 556 21. D. Hesterberg and A. Page, *Soil Science Society of America Journal*, 1990, **54**, 735-739.
- 557 22. L. Cai, M. Tong, X. Wang and H. Kim, *Environmental science & technology*, 2014, **48**,
558 7323-7332.
- 559 23. H. J. Kim, T. Phenrat, R. D. Tilton and G. V. Lowry, *Journal of colloid and interface*
560 *science*, 2012, **370**, 1-10.
- 561 24. M. E. Essington, J. Lee and Y. Seo, *Soil Science Society of America Journal*, 2010, **74**,
562 1577.
- 563 25. X. Gu and L. J. Evans, *Journal of colloid and interface science*, 2007, **307**, 317-325.
- 564 26. R. Hunter, *Foundations of colloid science*, Oxford University Press, Oxford, 2001.
- 565 27. J. W. Virden and J. C. Berg, *Journal of colloid and interface science*, 1992, **149**, 528-535.

- 566 28. A. Panáček, L. Kvitek, R. Prucek, M. Kolar, R. Vecerova, N. Pizurova, V. K. Sharma, T.
567 j. Nevečná and R. Zboril, *The Journal of Physical Chemistry B*, 2006, **110**, 16248-16253.
- 568 29. L. L. Schramm and J. C. T. Kwak, *Clays and Clay Minerals*, 1982, **30**, 40-48.
- 569 30. S. Garcia-Garcia, S. Wold and M. Jonsson, *Journal of colloid and interface science*, 2007,
570 **315**, 512-519.
- 571 31. E. Tombácz, J. Balázs, J. Lakatos and F. Szántó, *Colloid and Polymer Science*, 1989, **267**,
572 1016-1025.
- 573 32. A. Delgado, F. Gonzalez-Caballero and J. Bruque, *Journal of colloid and interface*
574 *science*, 1986, **113**, 203-211.
- 575 33. V. Metz, K. Amram and J. Ganor, *Geochim. Cosmochim. Acta*, 2005, **69**, 1755-1772.
- 576 34. P. Leroy, C. Tournassat, O. Bernard, N. Devau and M. Azaroual, *Journal of colloid and*
577 *interface science*, 2015, **451**, 21-39.
- 578 35. E. E. Saka and C. Güler, *Clay Minerals*, 2006, **41**, 853-861.
- 579 36. Y. Horikawa, R. Murray and J. Quirk, *Colloids and surfaces*, 1988, **32**, 181-195.
- 580 37. I. Callaghan and R. Ottewill, *Faraday Discussions of the Chemical Society*, 1974, **57**,
581 110-118.
- 582 38. S. Rossi, P. F. Luckham and T. F. Tadros, *Colloids and Surfaces A: Physicochemical and*
583 *Engineering Aspects*, 2002, **201**, 85-100.
- 584 39. I. Sondi, J. Bišćan and V. Pravdić, *Journal of colloid and interface science*, 1996, **178**,
585 514-522.
- 586 40. N. R. O'Brien, *Clays and Clay Minerals*, 1971, **19**, 353-359.
- 587 41. L. B. Williams and R. L. Hervig, *American Mineralogist*, 2002, **87**, 1564-1570.
- 588 42. J. Hower and T. C. Mowatt, *American Mineralogist*, 1900, **51**.
- 589 43. K. A. Huynh and K. L. Chen, *Environmental science & technology*, 2011, **45**, 5564-5571.
- 590 44. A. M. El Badawy, K. G. Scheckel, M. Suidan and T. Tolaymat, *Science of the Total*
591 *Environment*, 2012, **429**, 325-331.
- 592 45. B. Derjaguin and L. Landau, *Acta Physicochim. URSS*, 1941, **14**, 633-652.
- 593 46. E. J. W. Verwey and J. T. G. Overbeek, *Theory of the stability of lyophobic colloids*,
594 Courier Dover Publications, 1999.
- 595 47. J. Oster, I. Shainberg and J. Wood, *Soil Science Society of America Journal*, 1980, **44**,
596 955-959.

- 597 48. H. Van Olphen and P. H. Hsu, *Soil Science*, 1978, **126**, 59.
- 598 49. A. Katz, M. Xu, J. C. Steiner, A. Trusiak, A. Alimova, P. Gottlieb and K. Block, *Clays*
599 *and Clay Minerals*, 2013, **61**, 1-10.
- 600 50. H. Arora and N. Coleman, *Soil Science*, 1979, **127**, 134-139.
- 601 51. P. Rengasamy, *Journal of soil science*, 1983, **34**, 723-732.
- 602 52. R. Greene, A. Posner and J. Quirk, *Journal*.
- 603 53. M. Alvarez-Silva, A. Uribe-Salas, M. Mirnezami and J. Finch, *Minerals Engineering*,
604 2010, **23**, 383-389.
- 605 54. E. Errais, J. Duplay, M. Elhabiri, M. Khodja, R. Ocampo, R. Baltenweck-Guyot and F.
606 Darragi, *Colloids and Surfaces A: Physicochemical and Engineering Aspects*, 2012, **403**, 69-78.
- 607 55. Y. Lan, B. Deng, C. Kim and E. C. Thornton, *Geochemical transactions*, 2007, **8**, 4.
- 608 56. M. Muneer and J. Oades, *Soil Research*, 1989, **27**, 411-423.
- 609 57. Y. Mao, M. Cates and H. Lekkerkerker, *Physica A: Statistical Mechanics and its*
610 *Applications*, 1995, **222**, 10-24.
- 611 58. B. Götzelmann, R. Evans and S. Dietrich, *Physical Review E*, 1998, **57**, 6785.
- 612 59. M. Elimelech, X. Jia, J. Gregory and R. Williams, *Particle deposition & aggregation:*
613 *measurement, modelling and simulation*, Butterworth-Heinemann, 1998.
- 614 60. Y. Liang, S. A. Bradford, J. Simunek, M. Heggen, H. Vereecken and E. Klumpp,
615 *Environmental science & technology*, 2013, **47**, 12229-12237.
- 616 61. V. G. Pol, D. Srivastava, O. Palchik, V. Palchik, M. Slifkin, A. Weiss and A. Gedanken,
617 *Langmuir : the ACS journal of surfaces and colloids*, 2002, **18**, 3352-3357.

618

619

Table 1. Estimated Critical coagulation concentration (CCC) of suspensions in different electrolyte types

Particle type	CCC (mM)		
	NaCl	NaNO ₃	CaCl ₂
Bare silver nanoparticles	40	35	2
Na-MONT	50	50	1.5
Ca-MONT	50	50	2
Na-Illite	70	70	2
Ca-Illite	50	50	1

Figure Captions

Figure 1. Zeta potential of montmorillonite and illite from pH 4 to 10 in systems with 1mM NaCl.

Figure 2. Zeta potential of (a) montmorillonite and (b) illite in the systems with 1 – 500 mM NaCl or 0.1 – 10 mM CaCl₂.

Figure 3. Aggregation profiles of silver nanoparticles at pH 7.0 as a function of electrolyte concentrations in (a) NaCl and (b) NaNO₃.

Figure 4. Inverse stability ratio (1/W) of silver nanoparticles as a function of NaCl, NaNO₃ and CaCl₂ concentration. The arrows indicate the CCCs for the different systems.

Figure 5. Inverse stability ratio (1/W) of (a) Na-montmorillonite and (b) Ca-montmorillonite as a function of NaCl, NaNO₃ and CaCl₂ concentrations. The arrows indicate the CCCs for the different systems.

Figure 6. Inverse stability ratio (1/W) of (a) Na-illite and (b) Ca-illite as a function of NaCl, NaNO₃ and CaCl₂ concentrations. The arrows indicate the CCCs for different systems.

Figure 7. Inverse stability ratio (1/W) of silver nanoparticles with Na-montmorillonite (left)/Ca-montmorillonite (right) as a function of electrolyte concentrations: NaCl (a and d), NaNO₃ (b and e) and CaCl₂ (c and f). The arrows indicate the CCCs for different systems.

Figure 8. TEM image of heteroaggregated silver nanoparticles with Na-montmorillonite at 100mM NaCl. Red circles highlight the interactions between AgNPs and basal planes of Na-montmorillonite.

Figure 9. Inverse stability ratio (1/W) of silver nanoparticles with Na-illite (left)/Ca-illite (right) as a function of electrolyte concentrations: NaCl (a and d), NaNO₃ (b and e) and CaCl₂ (c and f). The arrows indicate the CCCs for different systems.

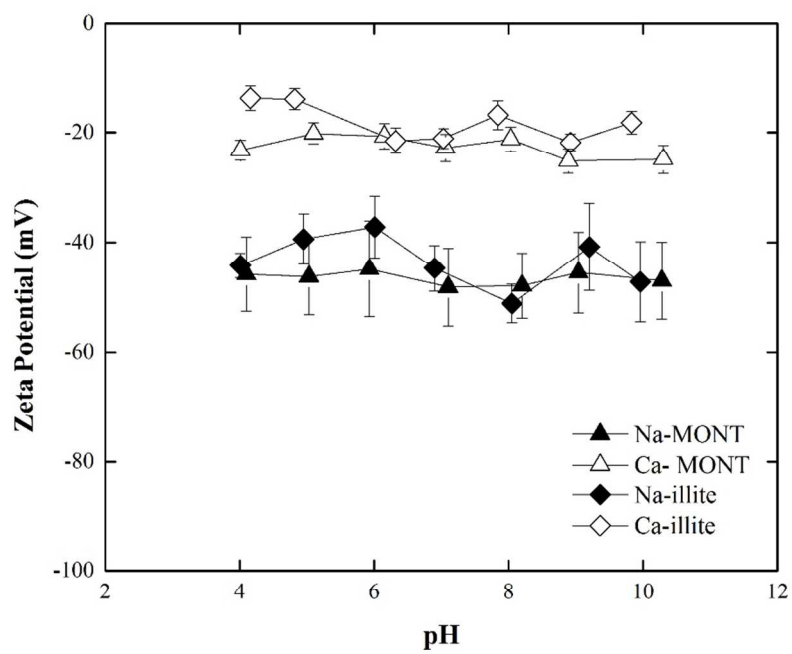


Figure 1.

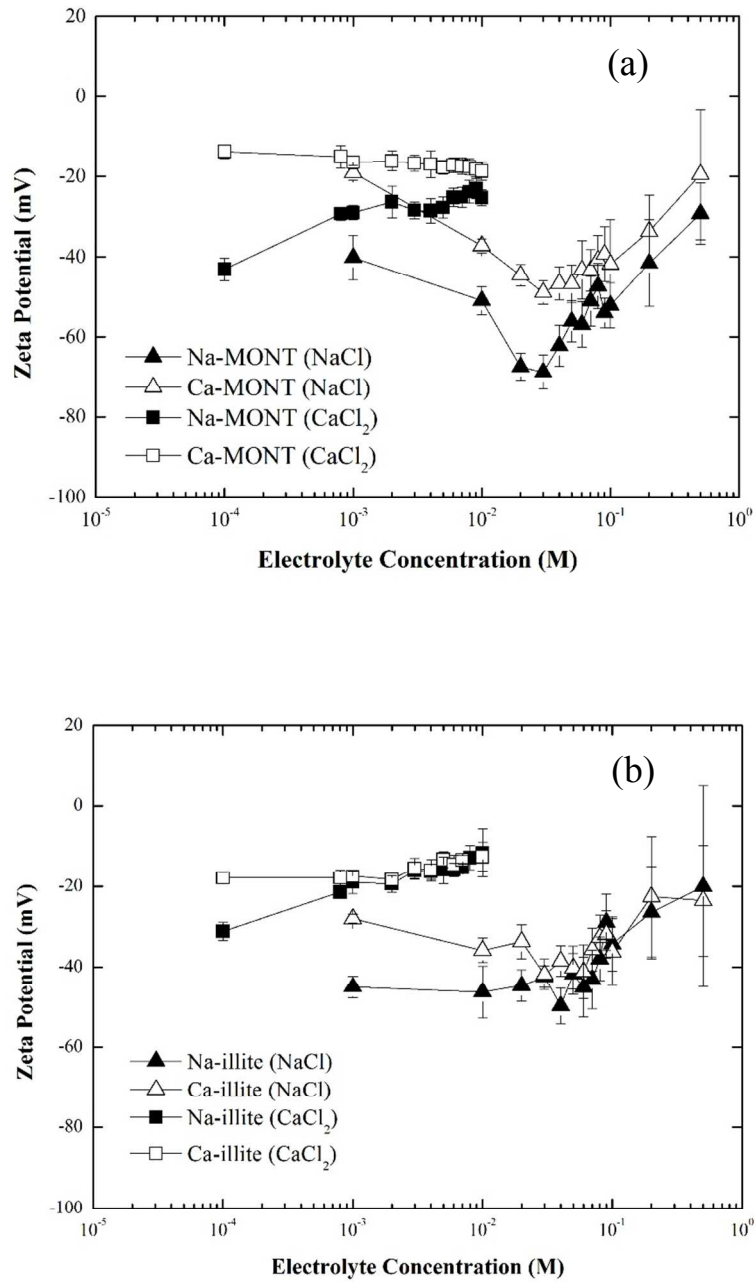


Figure 2.

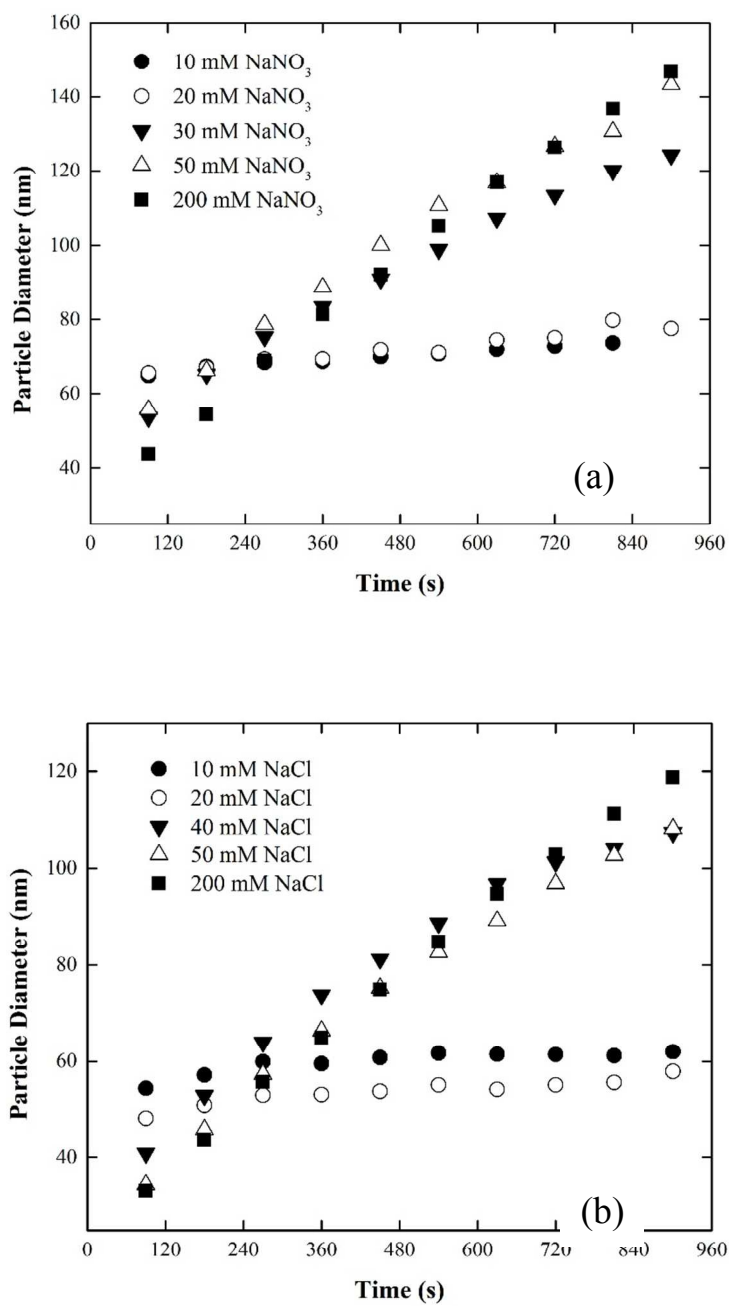


Figure 3.

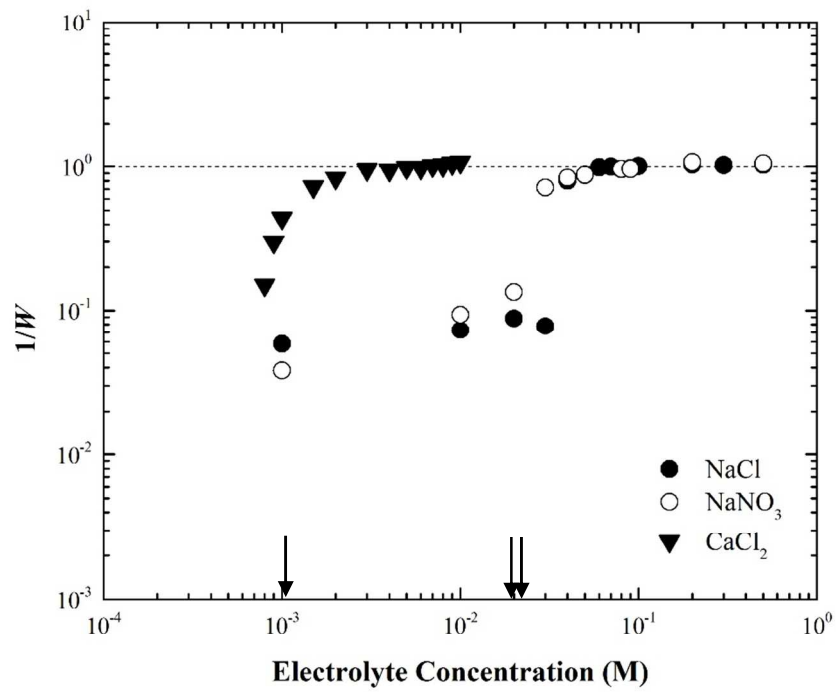


Figure 4.

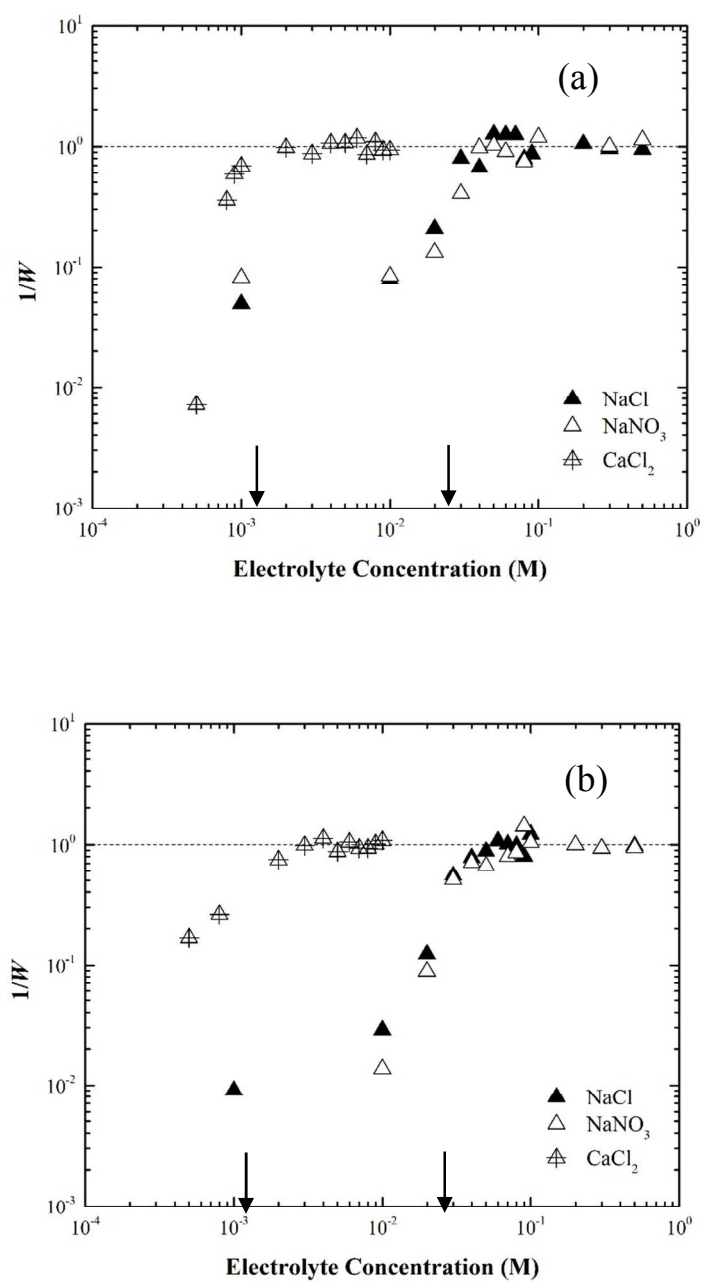


Figure 5.

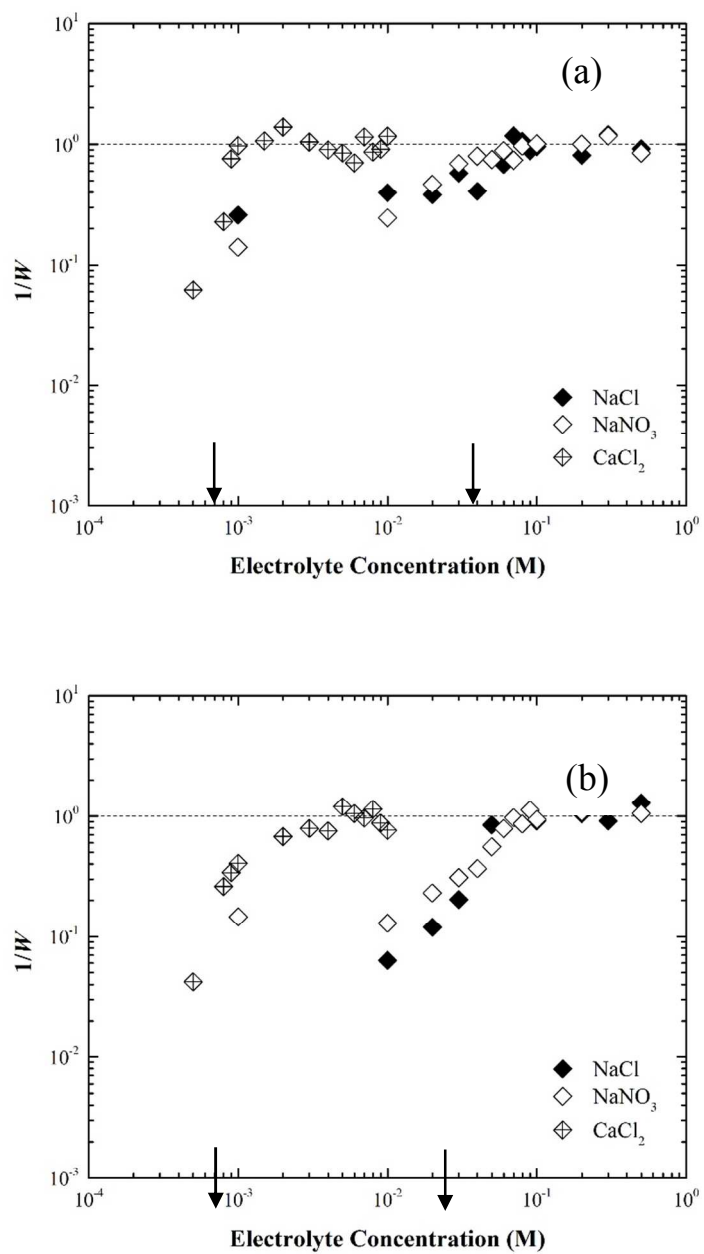


Figure 6.

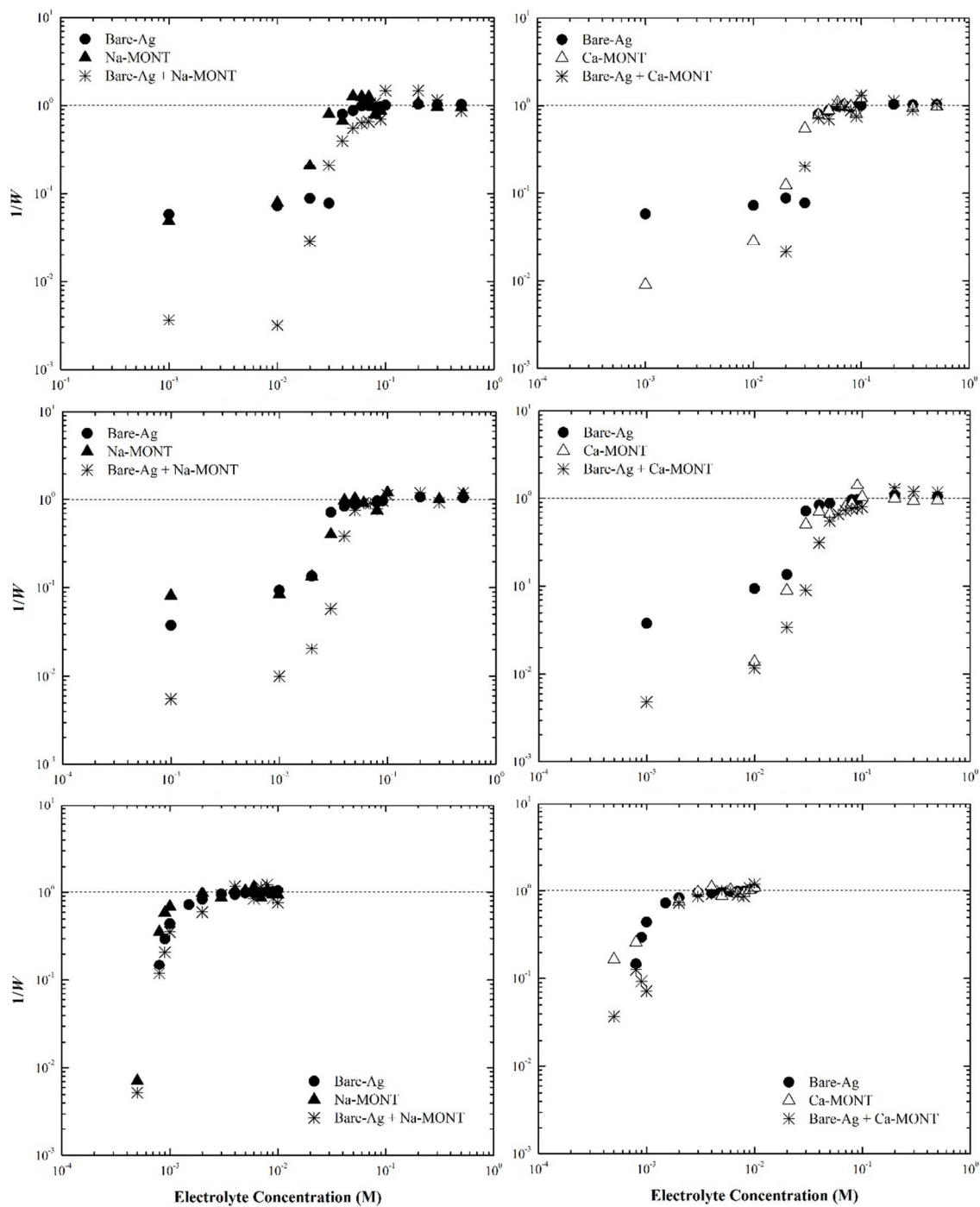


Figure 7.

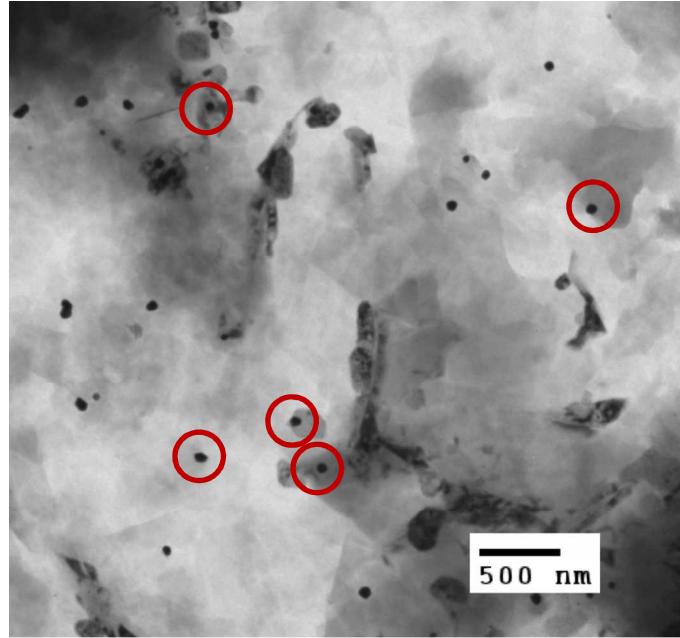


Figure 8.

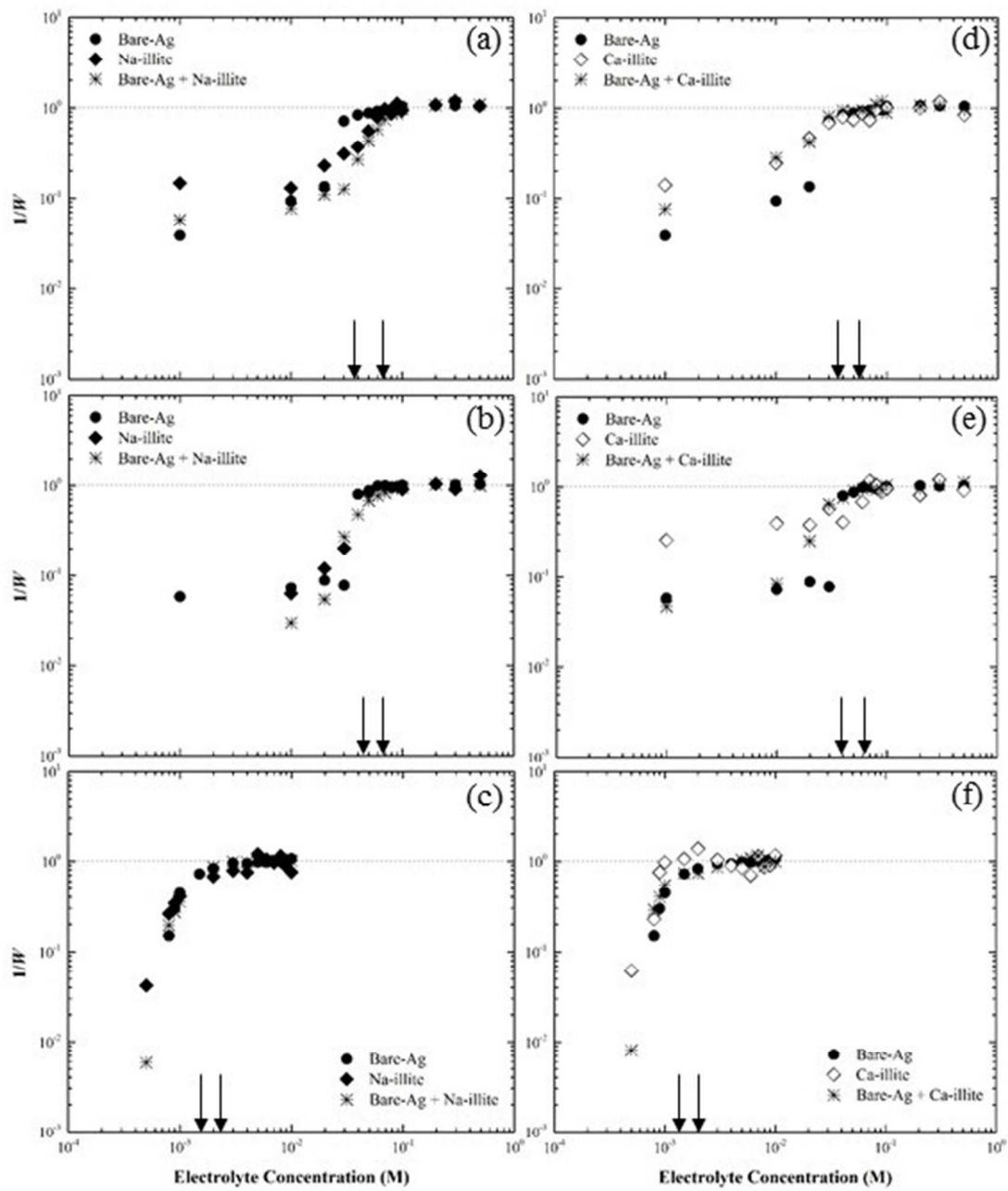


Figure 9.